ELSEVIER

Journal of Organometallic Chemistry 550 (1998) 315–329

Journal of Organometallic Chemistry

Rhodathiaboranes with 'anomalous' electron counts: synthesis, structure and reactivity [1]

Kerry J. Adams [a], Thomas D. McGrath [a], Georgina M. Rosair [b], Andrew S. Weller [b], Alan J. Welch [a,b,*]

[a] *Department of Chemistry, University of Edinburgh, Edinburgh, EH9 3JJ, UK*
[b] *Department of Chemistry, Heriot-Watt University, Edinburgh, EH14 4AS, UK*

Received 10 March 1997

Abstract

Analysis of the structures of 8,8-$(PPh_3)_2$-8,7-*nido*-$RhSB_9H_{10}$ and 9,9-$(PPh_3)_2$-9,7,8-*nido*-$RhC_2B_8H_{11}$ by RMS misfit calculations has confirmed that these rhodaheteroboranes possess *nido* 11-vertex cluster geometries in apparent contravention of Wade's rules. However, examination of the molecular structures of both species shows that the {RhP_2} planes are inclined by ca. 66° with respect to the metal-bonded SB_3 or CB_3 faces, and that two weak *ortho*-CH · · · Rh agostic interactions occupy the vacant co-ordination position thereby created. As a consequence of these agostic bonds the Rh atom, and hence the overall cluster, is provided with an additional electron pair, meaning that their *nido* structures are now fully consistent with Wade's rules. The chelated diphosphine compound 8,8-(dppe)-8,7-*nido*-$RhSB_9H_{10}$ is similar to the PPh_3 compound in showing the same agostic bonding. Attempts to prepare a bis-$P(OMe)_3$ analogue result in ligand scavenging and the formation of 8,8,8-{$P(OMe)_3$}$_3$-8,7-*nido*-$RhSB_9H_{10}$. Similarly, reaction between Cs[6-*arachno*-SB_9H_{12}] and RhCl(dmpe)CO does not result in CO loss but in formation of 8,8-(dmpe)-8-(CO)-8,7-*nido*-$RhSB_9H_{10}$, shown to exist as a mixture of two of three possible rotamers. Deprotonation of 8,8-$(PPh_3)_2$-8,7-*nido*-$RhSB_9H_{10}$ and 8,8-(dppe)-8,7-*nido*-$RhSB_9H_{10}$ with MeLi yields the anions [1,1-$(PPh_3)_2$-1,2-*closo*-$RhSB_9H_9]^-$ and [1,1-dppe-1,2-*closo*-$RhSB_9H_9]^-$, respectively, with octadecahedral cage structures. It is argued that anion formation causes the agostic bonding to be 'switched-off' and results in the cluster adopting the closo architecture predicted by Wade's rules. This structural change is fully reversible on reprotonation, and if reprotonation of [1,1-(dppe)-1,2-*closo*-$RhSB_9H_9]^-$ is carried out in MeCN, the product 8,8-(dppe)-8-(MeCN)-8,7-*nido*-$RhSB_9H_{10}$ forms. Interestingly, 8,8-(dppe)-8-(MeCN)-8,7-*nido*-$RhSB_9H_{10}$ reconverts to 8,8-(dppe)-8,7-*nido*-$RhSB_9H_{10}$ on standing in $CDCl_3$, suggesting that the agostic bonding is sufficiently strong to displace co-ordinated MeCN. All new compounds are fully characterised by multinuclear NMR spectroscopy and, in many cases, by single crystal X-ray diffraction. © 1998 Elsevier Science S.A.

Keywords: Rhodathiaboranes; Wade's rules; NMR spectroscopy; X-ray diffraction

1. Introduction

It is now more than 25 years since the publication of Ken Wade's seminal communication describing the relationship between structure and electron count in cluster compounds that became known as 'Wade's rules' [1]. The impact of these rules and their importance to the area can be judged by the fact that they are still widely employed today, and derive from the fact that the rules have their basis in molecular orbital theory. It is therefore of considerable interest when exceptions to the rules are reported. Two such compounds are the rhodathiaborane 8,8-$(PPh_3)_2$-8,7-*nido*-$RhSB_9H_{10}$ (**1**) [2,3] and its derivative 8,8-$(PPh_3)_2$-9-(OEt)-8,7-*nido*-$RhSB_9H_9$ [4]. These compounds appear, on first inspection, to have only 12 skeletal electron pairs (SEPs), yet display the *nido* 11-vertex geometries usually associated with an SEP count of 13. We were intrigued by the results of Ferguson et al. and Murphy et al. reported in Refs. [2–4], and the possibility that there might be an alternative explanation for the structures of these 'rule-breaking' molecules.

In this paper we report the results of root-mean-square (RMS) misfit calculations [5] on these 'anomalous' rhodathiaboranes. We show that, geometrically, the 11-vertex cages of these compounds *are* best described as *nido* 11-vertex, but we identify the presence of an unusual source of an extra SEP that accounts for their

* Corresponding author.
[1] Dedicated to Professor Ken Wade on the occasion of his 65th birthday.

structures within the framework of Wade's rules. We report the results of attempts to prepare analogues that are denied this additional SEP and the structural consequences of simple deprotonation of the 'rule breakers'. A preliminary account of some of this work has already appeared [6].

2. Experimental

2.1. Synthesis

2.1.1. General

All experiments were carried out under a dry, oxygen-free dinitrogen atmosphere, using standard Schlenk techniques. Solvents were dried over the appropriate drying agents and distilled immediately prior to use (CH_2Cl_2, CaH_2; THF and diethylether, Na wire/benzophenone; toluene and 60–80°C light petroleum fractions, Na wire). Chromatography columns (3×15 cm) were packed with silica (Kieselgel 60, 200–400 mesh). $[RhCl(\eta^2,\eta^2\text{-}C_8H_{12})]_2$ [7], $[RhCl(CO)_2]_2$ [8], $[RhCl(\eta\text{-}C_2H_4)_2]_2$ [9], $Cs[SB_9H_{12}]$ [10] and **1** [2,3] were prepared by published procedures or slight variants thereof.

2.1.2. NMR spectroscopy

^1H NMR spectra were recorded on a Bruker AC 200 spectrometer and ^1H, ^{11}B and ^{31}P spectra on a Bruker DPX 400 spectrometer. Measurements were recorded at 297 K in $CDCl_3$ solutions unless otherwise stated. Proton chemical shifts are reported relative to residual protio solvent in the sample, ^{11}B relative to external $BF_3 \cdot OEt_2$ at 128.0 MHz and ^{31}P relative to external H_3PO_4 at 162.0 MHz. All chemical shifts (δ) are reported as ppm and coupling constants given in Hertz.

2.1.3. Infrared Spectroscopy

Infrared spectra were recorded from CH_2Cl_2 solutions, using 0.1 mmol NaCl solution cells on a Nicolet Impact 400 FTIR spectrophotometer.

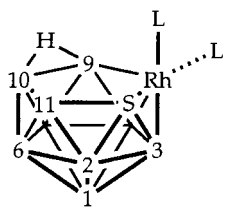

	L,L
1	PPh_3, PPh_3
2	dppe

2.2. 8,8-(dppe)-8,7-nido-$RhSB_9H_{10}$ (2)

To a suspension of $[RhCl(\eta\text{-}C_2H_4)_2]_2$ (0.100 g, 0.26 mmol) in toluene (10 cm^3) was slowly added a solution of dppe (dppe = diphenylphosphinoethane) (0.210 g, 0.52 mmol) in the same solvent (7 cm^3). The mixture was stirred for 22 h then frozen to 77 K. Solid Cs[6-*arachno*-SB_9H_{12}] (0.140 g, 0.52 mmol) was added and the reaction mixture warmed to room temperature and stirred for a further 5 h to afford a red–brown solution. Filtration through a Celite pad followed by removal of the solvent yielded the crude product as an orange powder. Thin layer chromatography, eluting with CH_2Cl_2:petroleum ether, 3:2, afforded a single mobile orange band of 8,8-(dppe)-8,7-*nido*-$RhSB_9H_{10}$, mass 0.154 g, yield 56%. $C_{26}H_{34}B_9P_2RhS$ requires C 48.7, H 5.35%. Found for **2**: C, 49.2; H, 5.10%. $^{31}P\{^1H\}$ NMR: 58.7 [br d, J(RhP) 139]; $^{31}P\{^1H\}$ NMR (223 K): 67.08 [dd, J(PP) 25, J(RhP) 142], 51.05 [dd, J(PP) 25, J(RhP) 133]; $^{11}B\{^1H\}$ NMR (CD_2Cl_2): 10.0 [br, 3B], −7.3 [2B], −11.6 [3B], −26.1 [1B]; ^1H NMR: 7.53 − 7.31 [m, 20H, Ph], 2.90 − 2.76 [br m, 2H, CH_2], 2.42 − 2.30 [br m, 2H, CH_2]; IR: 2545 [m br, B–H] cm^{-1}.

2.3. 8,8,8-{$P(OMe)_3$}$_3$-8,7-nido-$RhSB_9H_{10}$ (3)

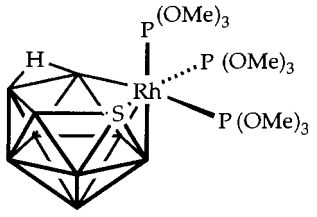

3

$[RhCl(\eta^2,\eta^2\text{-}C_8H_{12})]_2$ (0.180 g, 0.36 mmol) was dissolved in CH_2Cl_2 (10 cm^3). To this solution was added $P(OMe)_3$ (1.44 mmol in 1 cm^3) over 2 min via syringe, and the reaction mixture stirred for 2 h at room temperature. Volatiles were removed in vacuo and the resulting yellow solid redissolved in THF (10 cm^3) and cooled to 77 K. Solid Cs[6-*arachno*-SB_9H_{12}] (0.220 g, 0.80 mmol) was added and the reaction mixture warmed to room temperature and stirred for a further 2 h to afford a red–brown solution. Solvent was removed in vacuo and the residue redissolved in CH_2Cl_2 (10 cm^3) and filtered through a Celite pad. Concentration of the filtrate to ca. 2 cm^3 and subsequent thin layer chromatography, eluting with neat CH_2Cl_2, afforded a single mobile bright yellow band. Recrystallisation from CH_2Cl_2–petroleum ether afforded yellow 8,8,8-{$P(OMe)_3$}$_3$-8,7-*nido*-$RhSB_9H_{10}$, mass 0.206 g, yield 42%. $C_9H_{37}B_9O_9P_3RhS$ requires C 17.6, H 6.07%. Found for **3**: C, 17.1; H, 5.81%. $^{31}P\{^1H\}$ NMR: 141.6 [ddd, J(PP) 57, 70, J(RhP) 205], 125.2 [ddd, J(PP) 14, 70, J(RhP) 195], 121.9 [v br d, J(RhP) 129]; ^{11}B NMR: 15.1 [1B, J(HB) 128], 5.35 [v br, 2B], 3.84 [1B, J(HB) 134.4], 0.30 [1B, J(HB) 133], −13.06 [1B, J(HB) 155], −14.24 [1B, J(HB) 142, J(RhB) ca. 30], −21.2 [1 B, J(HB) 137, J(RhB) ca. 30], −25.9 [br, 1B, J(HB) 139]; ^1H NMR: 3.71 [d, 9 H, OMe, J(PH) 11], 3.62 [app d, 18 H, OMe, J(PH) 12].

2.4. 8,8-(dmpe)-8-(CO)-8,7-nido-$RhSB_9H_{10}$ (4)

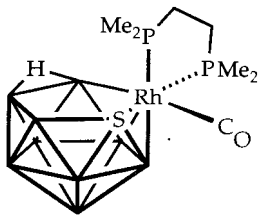

4

$[RhCl(CO)_2]_2$ (0.100 g, 0.258 mmol) was dissolved in toluene (10 cm^3). To this was added dmpe (dmpe = dimethylphosphinoethane) (2 equiv.), resulting in the precipitation of a yellow solid. The solution was stirred for a further hour at room temperature. Toluene was removed in vacuo and the resulting solid redissolved in CH_2Cl_2 and frozen to 77 K. Cs[6-*arachno*-SB_9H_{12}] (0.142 g, 0.517 mmol) was added and the reaction warmed to room temperature, with stirring, over 18 h. The resulting solution was filtered through a Celite pad and reduced in volume in vacuo to ca. 4 cm^3. This was chromatographed (silica, CH_2Cl_2:light petrol, 7:3) to afford a minor yellow band (see results and discussion) and a major orange band of 8,8-(dmpe)-8-(CO)-8,7-*nido*-$RhSB_9H_{10}$, mass 0.121 g, yield 52%. $C_8H_{26}B_9O_2P_2RhS$ requires C 21.4, H 5.84%. Found for **4**: C, 21.0; H 6.38%. $^{31}P\{^1H\}$ NMR: (mixture of isomers 48.2 [d, *J*(RhP) 119], 45.3 [br d, *J*(RhP) 118], 29.5 and 28.8 [overlapping d]. $^{11}B\{^1H\}$ NMR: (mixture of isomers), peaks at 14.1, 13.2, 5.44, 0.19, −15.5, −15.9, −16.8, −21.3, −22.1, −23.0, −23.8, −28.5; ^1H NMR: (mixture of isomers) 2.25 − 1.45 [br m, dmpe]; IR: 2530 [m br, B–H], 2039 [vs, C–O] cm^{-1}.

2.5. [PPN][1,1-(dppe)-1,2-closo-$RhSB_9H_9$], [PPN]**5**

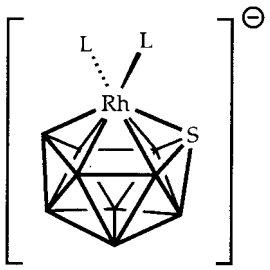

L,L	
5	dppe
6	PPh_3, PPh_3

Compound **2** (0.05 g, 0.078 mmol) was dissolved in THF (5 cm^3) and cooled to 195 K. MeLi (0.055 cm^3, 0.077 mmol) was added and the solution warmed slowly to room temperature. [PPN]Cl [PPN = $(Ph_3P)_2N$] (0.050 g, 0.087 mmol) was then added and the reaction mixture stirred for a further 1 h. The solvent was removed in vacuo and the resulting solid redissolved in CH_2Cl_2 and filtered through a Celite pad. The volume of the filtrate was reduced to ca. 2 cm^3 and light petroleum (5 cm^3) added, resulting in precipitation of an orange solid. The supernatant was removed via syringe and the product washed in diethyl ether (5 cm^3) and dried in vacuo to afford 0.075 g, 82% yield of [PPN][1,1-(dppe)-1,2-*closo*-$RhSB_9H_9$]. $C_{62}H_{63}B_9NP_4RhS$ requires C 63.2, H 5.39%. Found for [PPN]**5**: C, 63.8; H, 6.22%.; $^{31}P\{^1H\}$ NMR (CD_3CN): 69.4 [d, *J*(RhP) 155]; $^{11}B\{^1H\}$ NMR (CD_3CN): 58.6 [1 B], 28.3 [1 B], 4.6 [br, 2 B], −9.9 [1 B], −24.4 [2 B], −29.5 [2 B]; ^1H NMR (CD_3CN): 7.90 [br m, 4 H, Ph], 7.68 − 7.25 [m, 46 H, Ph], 2.40 [m, 4 H, CH_2].

2.6. [Li(12-crown-4)$_2$][1,1-(dppe)-1,2-closo-$RhSB_9H_9$], [Li(12-crown-4)$_2$]**5**

In a similar manner to that described for [PPN]**5**, compound **2** (0.05 g, 0.078 mmol) was deprotonated with MeLi (0.055 cm^3, 0.078 mmol) in THF (5 cm^3). After warming to room temperature 12-crown-4 (0.030 cm^3, 0.156 mmol) was added. The solution was stirred for 1 h and the volume reduced in vacuo by ca. half. Addition of 0.5 cm^3 light petroleum afforded orange microcrystals of [Li(12-crown-4)$_2$][1,1-(dppe)-1,2-*closo*-$RhSB_9H_9$], mass 0.071 g, yield 92%. $C_{42}H_{65}B_9LiO_8P_2RhS$ requires C 50.5, H 6.56%. Found for [Li(12-crown-4)$_2$]**5**: C, 50.1; H, 5.74%. ^{11}B and ^{31}P NMR spectra are essentially identical to that reported for [PPN]**5**; ^1H NMR (CD_2Cl_2): 7.71 [br m, 3 H, Ph], 7.38 [m, 5 H, Ph], 7.20 [br m, 12 H, Ph], 3.59 [s, 32 H, 12-crown-4], 2.22 [m, 4 H, CH_2].

2.7. [BTMA][1,1-(PPh_3)$_2$-1,2-closo-$RhSB_9H_9$], [BTMA]**6**

Compound **1** (0.030 g, 0.047 mmol) was dissolved in THF (5 cm^3) and cooled to 195 K. MeLi (0.033 cm^3, 0.047 mmol) was added and the solution warmed slowly to room temperature. [BTMA]Cl (BTMA = $PhCH_2NMe_3$) (0.010 g, 0.054 mmol) was added and the reaction mixture stirred for a further 1 h. The solvent was removed in vacuo and the resulting solid redissolved in CH_2Cl_2 and filtered through a Celite pad. The volume was reduced to ca. 2 cm^3 and light petroleum (5 cm^3) added resulting in precipitation of an orange solid. The supernatant was removed via syringe and the product washed in diethyl ether (5 cm^3) and dried in vacuo to afford 0.028 g, 65% yield of [BTMA][1,1-(dppe)-1,2-*closo*-$RhSB_9H_9$]. Analytically pure [BTMA]**6** was never obtained, despite repeated attempts. $^{31}P\{^1H\}$ NMR (CD_2Cl_2): 44.9 [d, *J*(RhP) 154]; $^{11}B\{^1H\}$ NMR (CD_2Cl_2): 54.5 [1 B], 22.8 [1 B],

1.7 [br, 3 B], −25.1 [2 B], −31.7 [2 B]; ^{1}H NMR (CD_2Cl_2): 7.71 − 6.93 [br m, 35 H, Ph], 4.38 [s, 2 H, NCH_2], 3.01 [s, 9H, NMe_3].

2.8. 8,8-(dppe)-8-(MeCN)-8,7-nido-$RhSB_9H_{10}$ (7)

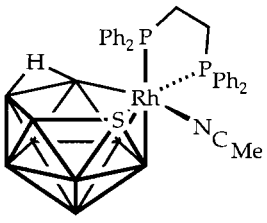

7

[Li(12-crown-4)$_2$]**5** (0.018 g, 0.018 mmol) was dissolved in MeCN (0.6 cm^3) and 10 μl CF_3CO_2H (15 equiv.) was added. There was an immediate colour change from orange to yellow, and, on standing, the solution deposited bright yellow diffraction quality crystals of 8,8-(dppe)-8-(MeCN)-8,7-*nido*-$RhSB_9H_{10}$. The supernatant was removed via syringe and the crystals washed in diethyl ether (2 × 2 cm^3) and dried in vacuo to afford 0.011 g, yield 87% of 8,8-(dppe)-8-(MeCN)-8,7-*nido*-$RhSB_9H_{10}$. $C_{28}H_{37}B_9NP_2RhS$ requires C 49.3, H 5.47%. Found for **7**; C, 50.0; H, 5.77%. ^{31}P{^{1}H} NMR: 69.5 [d br, *J*(RhP) 156], 50.9 [d br, *J*(RhP) 133]; ^{11}B{^{1}H} NMR (CD_3CN): 10.2 [2 B], 7.0 [2 B], 1.5 [1 B], −11.2 [1 B], −17.4 [1 B], −23.9 [1 B], −24.8 [1 B]; ^{1}H NMR: 7.32 [m, 20 H, Ph], 2.48 [s, 3 H, MeCN], 1.71 [br m, 4 H, CH_2].

2.9. X-ray crystallography

For **4**, intensity data at 150 K were collected on an Enraf–Nonius CAD4 diffractometer with a FAST detector by the EPSRC national crystallography service in Cardiff. Unit cell parameters were derived from 250 reflections and refined every 15° rotation in ω during data collection. Data reduction was performed using the program MADNES [11] and data were empirically corrected for absorption by DIFABS [12].

Measurements on [PPN]**5** and **7** were carried out at room temperature on a Siemens P4 diffractometer with graphite-monochromated Mo–Kα radiation (λ = 0.71069 Å) using ω scans. The unit cell parameters and

Table 1
Crystallographic data and details of refinement

Compound	**4**	[PPN]**5**	**7**
Formula	$C_7H_{26}B_9OP_2RhS$	$C_{63}H_{64.5}B_9N_{1.5}P_4RhS$[a]	$C_{30}H_{40}B_9P_2SRhN_2$[b]
M	420.48	1198.8[a]	722.84[b]
System	Monoclinic	Monoclinic	Monoclinic
Space group	$P2_1/n$	$P2_1/n$	$P2_1/n$
a/Å	10.559(2)	10.865(2)	10.261(1)
b/Å	14.007(3)	24.924(3)	17.075(2)
c/Å	12.552(3)	22.750(2)	21.326(2)
β/°	105.53(3)	92.797(9)	103.881(7)
U/Å^3	4091.9(12)	6153.6(13)	3627.3(9)
Z	4	4	4
D_{calc}/g cm^{-3}	1.561	1.294[a]	1.227[b]
μ(Mo–K$_\alpha$)/mm^{-1}	1.237	0.456[a]	0.641[b]
F(000)	848	2476[a]	1480[b]
2θ orientation/°	–	9.62 to 17.428	9.24 to 24.85
$\theta_{data\ collection}$/°	2.22 to 25.04	1.21 to 24.99	1.55 to 24.99
h range	$-11 \le h \le 11$	$-1 \le h \le 12$	$-1 \le h \le 12$
k range	$-15 \le k \le 11$	$-1 \le k \le 29$	$-1 \le k \le 20$
l range	$-13 \le l \le 13$	$-27 \le l \le 27$	$-25 \le l \le 25$
ω scan speeds/°min^{-1}	1.5, 35.0	2.0, 40.0	1.5, 60
Data measured	7417	13 054	8002
Unique data	2951	10 643	6328
a	0.0347	0.0621	0.0661
b	0.0	0.0	9.08
R, *wR*^{2} (all data)	0.0477, 0.0922	0.2476, 0.2168	0.1321, 0.2141
Obs. data [$I > 2\sigma(I)$]	2695	4110	3711
R, *wR*^{2} (obs. data)	0.0346, 0.0816	0.0823, 0.1390	0.0600, 0.1452
S	1.035	1.151	1.108
Variables	215	598	437
E_{max}, E_{min} (eÅ^{-3})	1.23, −0.506	0.695, −0.492	0.63, −0.48

[a] Includes 0.5 mol of MeCN solvate per mol of rhodathiaborane.
[b] Assumes 1 mol of MeCN solvate per mol of rhodathiaborane.

orientation matrix for data collection were determined by a least-squares refinement of the setting angles of 28 centred reflections, with 2θ ranging from 9–25°. Standard reflections were re-measured every 100 data, with crystal decays of 40% ([PPN]**5**) and 11% (**7**) found. Data were corrected for absorption by psi scans.

All structures were solved by direct and difference Fourier methods and refined by full-matrix least-squares against F^2 (except **4**, refinement against F) using the SHELXTL system [13] on a Pentium 90 MHz PC. Table 1 lists details of unit cell data, intensity data collection and structure refinement.

In all cases methyl, methylene and phenyl, H atom positions were calculated (C–H = 0.97 Å for CH_3 and CH_2, C–H = 0.93 Å for Ar–H) and treated as riding models with U_H 1.5, 1.2 and 1.2 times the bound carbon atom U_{eq} respectively.

In the case of compound **4** positions 7 and 9 of the cage are disordered, with that labelled S(7) being 64.5%S, 35.5%B, and that labelled B(9) being 35.5%S and 64.5%B. Cage H atoms were located and positionally refined, with $U_{cage\text{-}H}$ fixed at 0.08 Å^2. The μ-H atom was not located.

For [PPN]**5**, cage H atoms were set in idealised positions (1.1 Å from B on a radial extension) and allowed to ride on their bound boron atom, with $U_{cage\text{-}H}$ 1.2 U_{eq}. Phenyl rings were constrained to idealised geometries (C–C 1.39 Å, CCC angles 120°). A half-molecule of MeCN co-crystallises with [PPN]**5**, and carbon and nitrogen atoms of this solvate were refined with isotropic thermal parameters.

Table 2
Positional parameters and equivalent isotropic thermal parameters for non-H atoms in compound **4**

	x	y	z	$U_{(eq)}$
Rh(8)	1305(1)	7992(1)	2679(1)	12(1)
P(2)	−77(1)	6685(1)	2724(1)	15(1)
P(1)	−650(1)	8864(1)	2160(1)	15(1)
S(7)	1175(2)	7871(1)	775(1)	17(1)
B(7)	175(2)	7871(1)	775(1)	17(1)
B(9)	3087(2)	6893(2)	3123(2)	20(1)
S(9)	3087(2)	6893(2)	3123(2)	20(1)
O(1)	1843(3)	8884(2)	4965(3)	28(1)
C(1)	1620(4)	8518(3)	4128(4)	19(1)
C(2)	−901(5)	9732(3)	1061(4)	25(1)
C(3)	−1158(5)	9493(3)	3247(4)	26(1)
C(4)	−1971(4)	7980(3)	1671(4)	19(1)
C(5)	−1765(5)	7143(3)	2480(4)	22(1)
C(6)	−192(4)	5771(3)	1675(4)	20(1)
C(7)	241(5)	6005(3)	4001(4)	23(1)
B(1)	4067(6)	8362(4)	1753(5)	20(1)
B(2)	2844(6)	8156(4)	512(5)	25(1)
B(3)	2476(6)	8785(4)	1695(5)	19(1)
B(4)	3478(5)	8237(4)	2939(5)	18(1)
B(5)	4448(6)	7284(4)	2530(5)	23(1)
B(6)	3981(6)	7243(4)	1069(5)	20(1)
B(10)	3350(6)	6378(4)	1789(5)	20(1)
B(11)	2348(6)	6907(4)	525(5)	21(1)

In compound **7** cage H atoms were located but refined subject to constrained B–H distances of 1.1 Å (terminal H) or 1.2 Å (μ-H). For these atoms U_H was refined freely. The structure of **7** suffers from severely disordered MeCN solvate molecules lying in channels parallel to *a*. A sensible (in terms of refined U_{iso} values) model was achieved by the inclusion of 2.75 C atoms per molecule of **7** (it proved impossible to distinguish N).

In the final stages of refinement data were weighted such that $w^{-1} = [\sigma^2(F_o) + (aP)^2 + bP]$ where $P = [\max(F_o^2 \text{ or } 0) + 2F_c^2]/3$. Unless otherwise stated all non-H atoms were refined with anisotropic displacement parameters.

Tables 2–5 list positional and equivalent isotropic thermal parameters for the non-hydrogen atoms of compound **4**, [PPN]5.0.5 MeCN and compound **7** solvate, respectively. Complete atomic co-ordinates, thermal parameters and bond lengths and angles (except those involving H atoms) have been deposited with the Editor.

3. Results and discussion

3.1. RMS misfit calculations

The rhodathiaborane **1** [2,3], together with its 9-OEt analogue [4], appears to be an example of a heteroborane that disobeys Wade's rules in that it has a *nido* 11-vertex cage structure yet seemingly only 12 SEPs [skeletal electron contribution from $\{Rh(PPh_3)_2\}$ fragment = $v + x - 12 = 9 + 4 - 12 = 1e$]. In this respect, **1** is clearly related to the isostructural carbarhodaborane 9,9-$(PPh_3)_2$-9,7,8-*nido*-$RhC_2B_8H_{11}$ **8**, previously synthesised [14] and structurally characterised [15].

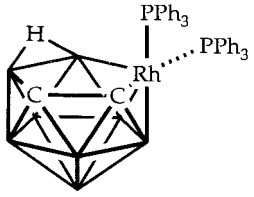

8

But are the cages of **1** and **8** really *nido*? Several years ago Barker et al. described formally *closo* carbaplatinaboranes with open structures [16], subsequently shown by Mingos et al. [17] to result from a mismatch of the frontier orbitals of carbaborane and metal–ligand fragments. Equally, we have recently demonstrated that formally *closo* carbametallaboranes can have partially opened (*pseudocloso*) structures where the origin of the opening is intramolecular steric crowding [18]. In both

Table 3
Positional parameters and equivalent isotropic thermal parameters for non-H atoms in [PPN]**5** · 0.5 MeCN

	x	*y*	*z*	$U_{(eq)}$
Rh(1)	5827(1)	7055(1)	−5002(1)	36(1)
S(2)	5456(3)	7724(1)	−5735(1)	64(1)
B(3)	4330(11)	6559(4)	−4716(5)	27(3)
B(4)	4708(13)	7052(5)	−5966(5)	53(4)
B(5)	4381(12)	7777(5)	−5084(5)	48(4)
B(6)	3915(12)	7222(5)	−4612(5)	47(4)
B(7)	4246(12)	6515(5)	−5477(5)	52(4)
B(8)	3657(14)	7637(5)	−5839(6)	65(4)
B(9)	3018(14)	6766(5)	−5048(6)	57(4)
B(10)	3158(14)	6983(5)	−5792(6)	64(4)
B(11)	2927(13)	7461(5)	−5215(5)	53(4)
P(1)	7534(3)	6589(1)	−5210(1)	39(1)
P(2)	7000(3)	7406(1)	−4261(1)	40(1)
C(1)	8755(10)	6722(4)	−4635(4)	46(3)
C(2)	8615(9)	7299(4)	−4395(4)	45(3)
C(11)	8272(7)	6760(3)	−5901(2)	45(3)
C(12)	7607(6)	6633(3)	−6419(3)	59(3)
C(13)	8068(9)	6768(3)	−6959(2)	85(5)
C(14)	9193(9)	7031(3)	−6981(3)	91(5)
C(15)	9857(6)	7159(3)	−6462(4)	80(4)
C(16)	9397(7)	7023(3)	−5922(3)	57(3)
C(21)	7576(7)	5857(2)	−5247(3)	34(3)
C(22)	8575(6)	5603(3)	−5486(3)	56(3)
C(23)	8626(6)	5046(3)	−5507(3)	63(4)
C(24)	7677(7)	4743(2)	−5288(3)	53(3)
C(25)	6678(6)	4996(2)	−5048(3)	44(3)
C(26)	6627(6)	5553(3)	−5028(2)	38(3)
C(31)	6897(7)	8138(2)	−4165(3)	43(3)
C(32)	7245(7)	8465(3)	−4623(3)	60(4)
C(33)	7131(8)	9019(3)	−4580(4)	79(4)
C(34)	6669(8)	9246(2)	−4078(4)	98(5)
C(35)	6321(8)	8919(3)	−3620(3)	121(7)
C(36)	6435(8)	8366(3)	−3663(3)	85(5)
C(41)	6901(8)	7161(3)	−3503(2)	46(3)
C(42)	5832(7)	6909(3)	−3335(3)	66(4)
C(43)	5712(7)	6763(3)	−2750(3)	81(4)
C(44)	660(9)	6870(3)	−2334(2)	70(4)
C(45)	7728(8)	7122(3)	−2503(3)	108(6)
C(46)	7849(7)	7268(3)	−3087(3)	89(5)
P(3)	1893(3)	10 023(1)	−3199(1)	39(1)
P(4)	4375(3)	10 453(1)	−2792(1)	42(1)
N(1)	3305(8)	10 088(3)	−3063(3)	46(2)
C(101)	1241(6)	10 537(2)	−3690(3)	41(3)
C(102)	627(7)	10 411(2)	−4222(3)	60(4)
C(103)	134(7)	10 817(4)	−4580(2)	76(4)
C(104)	255(8)	11 349(3)	−4406(3)	86(5)
C(105)	869(8)	11 476(2)	−3874(4)	75(4)
C(106)	1362(7)	11 070(3)	−3516(3)	67(4)
C(111)	1659(9)	9386(2)	−3548(3)	45(3)
C(112)	492(7)	157(3)	3599(3)	70(4)
C(113)	333(8)	8652(4)	−3850(4)	101(5)
C(114)	1342(11)	8376(2)	−4051(3)	96(6)
C(115)	2509(9)	8605(3)	−4000(3)	84(5)
C(116)	2667(7)	9110(3)	−3748(3)	71(4)
C(121)	1030(7)	10 031(3)	−2549(2)	38(3)
C(122)	8(8)	10 358(3)	−2488(3)	98(5)
C(123)	−587(7)	10 364(4)	−1961(4)	133(7)
C(124)	−160(9)	10 044(4)	−1495(3)	95(5)
C(125)	862(9)	9717(3)	−1555(3)	78(4)
C(126)	1457(7)	9711(3)	−2082(3)	64(4)
C(201)	5202(6)	10 110(3)	−2202(2)	42(3)
C(202)	5119(6)	9555(3)	−2163(3)	54(3)
C(203)	5766(7)	9283(2)	−1713(3)	65(4)

Table 3 (continued)

	x	y	z	$U_{(eq)}$
C(204)	6495(7)	9567(3)	−1301(3)	66(4)
C(205)	6578(6)	10 122(3)	−1340(3)	63(4)
C(206)	5931(7)	10 394(2)	−1791(3)	50(3)
C(211)	3899(7)	11 076(2)	−2480(3)	45(3)
C(212)	4122(6)	11 561(3)	−2759(3)	56(3)
C(213)	3704(8)	12 038(2)	−2524(4)	86(4)
C(214)	3063(8)	12 031(3)	−2010(4)	90(4)
C(215)	2839(7)	11 547(4)	−1731(3)	75(4)
C(216)	3257(7)	11 070(3)	−1966(3)	63(4)
C(221)	5396(7)	10 595(2)	−3370(3)	36(3)
C(222)	4874(6)	10 646(3)	−3937(3)	63(4)
C(223)	5614(8)	10 768(3)	−4401(2)	72(4)
C(224)	6874(8)	10 839(3)	−4297(3)	64(4)
C(225)	7396(6)	10 788(3)	−3729(3)	66(4)
C(226)	6656(7)	10 666(3)	−3266(2)	52(3)
C(301)	3356(23)	6236(9)	−7263(9)	71(7)
C(300)	4344(28)	6485(10)	−7447(10)	72(8)
N(2)	5210(25)	6695(9)	−7631(9)	107(8)

these latter cases the resulting open structure is probably better described as 'locally distorted *closo*' rather than true *nido*. Is this the case with **1** and **8**?

We have addressed this question by quantifying the shapes of the cages of **1** and **8** by RMS misfit calculations [5], the formal possibilities being that the cage is 11-vertex *nido* (fragment of an icosahedron) or 11-vertex *closo* (octadecahedron). Reference 11-vertex *nido* species taken from the literature were $[B_{11}H_{14}]^-$ **A** [19,20] and [7,8-$C_2B_9H_{12}]^-$ **B** [21], whereas $B_{10}H_{14}$ **C** [22] and [2-$(Me_3Si)_2$CH-2-$CB_{10}H_{10}]^-$ **D** [23] were selected as suitable 11-vertex *closo* models (in the case of **C** a *nido* fragment of a closed 11-vertex cage). Crystallographic co-ordinates of **B** and **D** were adjusted to C_s molecular symmetry and those of **C** (one crystallographically-independent molecule only) to C_{2v} symmetry; the 1997 determination of **A** already has crystallographically-imposed C_s symmetry. However, the differences in elements constituting the open faces (or upper fractions) of **1**, **8** and the model compounds **A**–**D**,

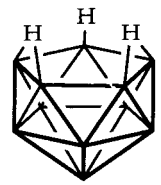

A

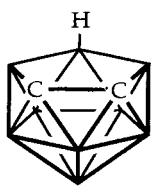

B

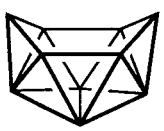

C

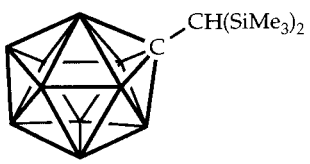

D

together with inconsistencies in the number and positions of μ-H atoms, requires that several cluster vertices must be omitted from the RMS misfit calculations, and the problem thereby reduces to a comparison of the pentagonal pyramidal fragments shown in **I** and **II**.

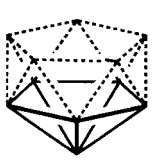

I

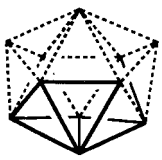

II

In Table 5a are given the overall misfit values between the pentagonal pyramidal fragments of **A**–**D**. The low values for *closo*/*closo* (**D**/**E**) and *nido*/*nido* (**A**/**B**) comparisons, and higher values for *closo*/*nido* comparisons (**A**/**C**, **A**/**D**, **B**/**C**, **B**/**D**) imply that the pentagonal pyramidal fragments of **I** and **II** can be distinguished by this method. Table 5b gives the overall misfit values obtained by fitting the appropriate pentagonal pyramidal fragments of **1** and **8** with those of the model polyhedra, from which it is immediately apparent that both **1** and **8** are truly *nido* species. [2]

However, we do not believe that they constitute exceptions to Wade's rules. Given that the 11-vertex species **1** and **8** are *nido* fragments of icosahedra, the metal-free 10 vertex subclusters $\{SB_9H_{10}\}$ and $\{C_2B_8H_{11}\}$ must consequently be *arachno* fragments of icosahedra, and both must therefore carry formal charges of −3. Thus, the formal rhodium oxidation state in **1**

[2] For a fuller account of the results of RMS misfit calculations in this area see Ref. [24].

Table 4
Positional parameters and equivalent isotropic thermal parameters for non-H atoms in compound **7**·solvate

	x	*y*	*z*	$U_{(eq)}$
P(1)	3408(2)	6735(1)	5667(1)	32(1)
N(1)	5141(9)	6092(5)	7107(4)	47(2)
C(1)	2168(10)	7500(6)	5702(4)	40(2)
B(1)	8508(11)	7841(7)	6716(5)	41(2)
P(2)	3873(2)	7818(1)	6901(1)	32(1)
C(2)	2166(9)	7620(6)	6410(4)	40(2)
B(2)	8685(10)	6945(8)	6350(5)	43(3)
C(3)	5003(14)	5609(8)	7427(7)	67(3)
B(3)	7552(10)	7060(8)	6930(5)	39(2)
B(4)	6838(9)	8022(7)	6778(5)	35(2)
C(4)	4761(29)	4960(13)	7852(12)	182(13)
B(5)	7425(13)	8463(6)	6144(6)	42(3)
B(6)	8509(10)	7799(8)	5879(5)	44(3)
S(7)	6959(3)	6359(2)	6107(1)	41(1)
Rh(8)	5319(1)	7086(1)	6472(1)	29(1)
B(9)	5743(10)	8099(6)	5952(5)	36(2)
B(10)	6894(9)	7941(8)	5390(5)	39(2)
B(11)	7681(10)	6968(8)	5522(5)	45(3)
C(11)	2584(10)	5820(6)	5784(4)	42(2)
C(12)	3382(12)	5139(7)	5939(6)	58(3)
C(13)	2815(15)	4439(7)	6017(6)	68(4)
C(14)	1468(16)	4375(7)	5969(7)	74(4)
C(15)	695(14)	5036(8)	5823(7)	70(4)
C(16)	1238(11)	5748(6)	5736(5)	48(2)
C(21)	3984(10)	8893(6)	6957(5)	40(2)
C(22)	4791(12)	9229(6)	7510(5)	52(3)
C(23)	4934(17)	10052(8)	7549(7)	82(4)
C(24)	4263(18)	10506(8)	7046(9)	93(5)
C(25)	3432(18)	10174(8)	6509(8)	88(5)
C(26)	3324(13)	9362(7)	6472(6)	60(3)
C(31)	3826(9)	7535(5)	7718(4)	37(2)
C(32)	2637(10)	7543(6)	7929(5)	44(2)
C(33)	2640(12)	7347(7)	8551(5)	55(3)
C(34)	3823(12)	7161(7)	8991(5)	54(3)
C(35)	5017(12)	7149(8)	8796(5)	58(3)
C(36)	5018(10)	7354(6)	8158(5)	47(2)
C(41)	3473(8)	6700(6)	4819(4)	39(2)
C(42)	3678(10)	7379(7)	4504(5)	53(3)
C(43)	3748(11)	7364(9)	3871(5)	70(4)
C(44)	3594(12)	6663(10)	3531(5)	72(4)
C(45)	3376(13)	5971(9)	3829(5)	67(3)
C(46)	3302(12)	6004(8)	4479(5)	56(3)
C(100)	12240(26)	9298(15)	4703(12)	134(8)
C(101)	13398(48)	9505(27)	4690(21)	120(14)
C(102)	14661(53)	9912(34)	4821(23)	132(16)
C(103)	11096(56)	9723(33)	4794(26)	156(19)
C(104)	10000	10000	5000	171(30)

and **8** is +3, an (internal) 2*e* redox change having accompanied the synthesis of **1** and **8**. Rh^{III}, d^6, typically has an octahedral co-ordination geometry [25], and bonds as an $\{ML_3\}$ conical fragment to η-bonded ligands like η^5-$[C_5H_5]^-$. Although it appears as though only an angular $\{ML_2\}$ fragment bonds to the η^4-$[SB_9H_{10}]^{3-}$ and η^4-$[C_2B_8H_{11}]^{3-}$ ligands in **1** and **8**, the '$\{ML_2\}$' plane [defined by Rh, P(1) and P(2)] is significantly tilted from orthogonal to the SB_3 and CB_3 ligand faces [Fig. 1a,b]. Moreover, in both cases two *ortho*-H atoms (one from each PPh_3 ligand) are located ca. 3 Å from Rh [Fig. 1c], with the mid-point of these H atoms, X, occupying the third site of what is now a *pseudo*-conical $\{RhP_2X\}$ metal fragment [Fig. 1d].

We suggest that these structural features imply the presence, in **1** and **8**, of two weak, nominally 1-*e* agostic bonds, designated as CH · · · Rh, which furnish the metal centre, and hence the overall cluster, with an additional electron pair. Thus, the skeletal electron contribution from the metal fragment is now $9 + 6 - 12 = 3e$, and the *nido* 11-vertex cage has 13 SEPs in accord with Wade's rules. Moreover the presence of these additional interactions increases the total number of valence electrons available to the Rh atom to 18.

Although agostic bonds usually emanate from formally saturated CH groups, several precedents exist for the involvement of *ortho*-CH units of aryl phosphines [26–30]. Only very recently, however, has the presence of 1-*e* agostic bonding been recognised [31,6], although it is likely that they also exist in several established compounds that have previously been described as having lower formal co-ordination geometries and electron counts, e.g., $RhI_2(CH_3)(PPh_3)_2$, classically a 5 co-ordinate 16-*e* compound [32], thus better described as 6 co-ordinate, 18-*e* (Fig. 2).

3.2. Attempts to prepare compounds denied agostic bonding

In order to test the supposition that the apparently anomalous geometries of **1** and **8** are due to weak agostic interactions from *ortho*-phenyl H atoms we attempted to utilise a $\{RhL_2\}$ fragment that could not agostically bond and yet still provide a 1-*e* overall contribution $(v + x - 12)$ to skeletal bonding. Initially we attempted the reactions between Cs[6-*arachno*-SB_9H_{12}] and $[Rh(L,L)Cl]_2$ [L,L = 1,5-cyclo-octadiene, norbornadiene, $(CO)_2$], but in all cases recovered only unidentified decomposition products. Although dppe is in many respects similar to $2 \times PPh_3$ it was possible that constraints in ligand stereochemistry imposed by the methylene backbone might disfavour the agostic interactions occurring in **1**. Reaction between $[Rh(dppe)Cl]_2$ [33] and Cs[6-*arachno*-SB_9H_{10}] followed by work-up involving chromatography afforded the compound 8,8-(dppe)-8,7-*nido*-$RhSB_9H_{10}$, **2**, as an orange crystalline material in moderate yield. The molecular structure of **2** (as two crystalline modifications) has been reported elsewhere [34,35], the relevant result being that **2**, like **1**, also has a *nido* structure involving two weak *ortho*-phenyl agostic interactions.

The room temperature $^{11}B\{^1H\}$ NMR spectrum of **2** displays four signals, in the ratio 3:2:3:1, between δ 10 and −27 ppm, the region associated with *nido*-MSB_9 fragments [2,3], whilst in the $^{31}P\{^1H\}$ NMR spectrum is

Table 5
(a) Overall RMS misfit values (Å) for comparison of the pentagonal pyramidal fragments of the model clusters **A**, **B**, **C** and **D** (**A**, **B** *nido* 11-vertex; **C**, **D** *closo* 11-vertex)

B	**C**	**D**	
0.016	0.110	0.084	**A**
	0.114	0.089	**B**
		0.063	**C**

(b) Overall RMS misfit values (Å) for comparison of the pentagonal pyramidal fragments of **1** and **8** with those of **A**–**D**

1/**A**	0.056
1/**B**	0.016
1/**C**	0.110
1/**D**	0.084
8/**A**	0.046
8/**B**	0.047
8/**C**	0.135
8/**D**	0.122

observed one broad doublet at δ 58.7 ppm [J(RhP) 139]. The ^{1}H NMR spectrum displays signals due to Ph and two multiplets, at δ 2.82 and δ 2.37 ppm, each of integral two, assigned to the dppe methylene backbone. Thus the NMR evidence suggests that **2** has C_s symmetry in solution, but yet a *nido* shielding pattern is observed in the ^{11}B spectrum and a *nido* structure is

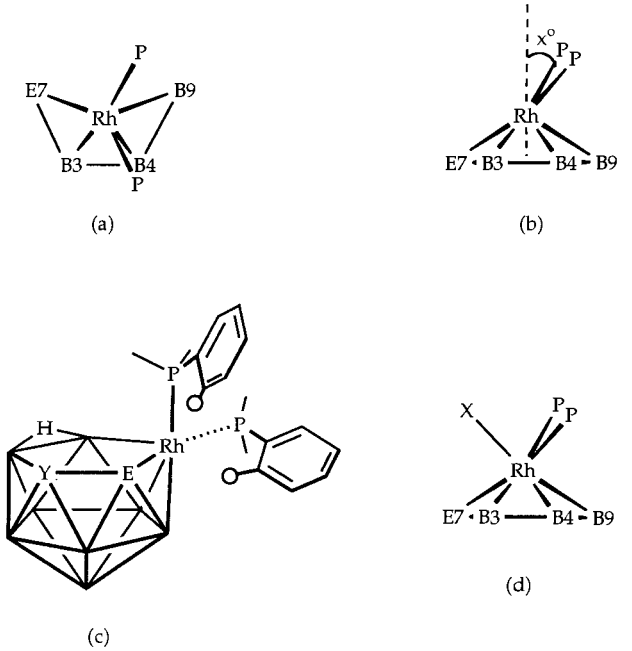

Fig. 1. (a) View of the {RhP_2} fragment of **1** and **8** projected onto the EB_3 face (E = S or C). (b) Side view showing the tilt of the {RhP_2} fragments (**1**, x = 66.6°; **8**, x = 65.4°). (c) Close approach of two *ortho*-H atoms to Rh (**1**, Rh…H = 2.995 and 3.007 Å; **8**, Rh…H = 2.768 and 2.987 Å). For **1**, Y = B; for **8** Y = C. (d) Complete rhodium co-ordination sphere, including x, the mid-point of the two closely approaching *ortho*-H atoms.

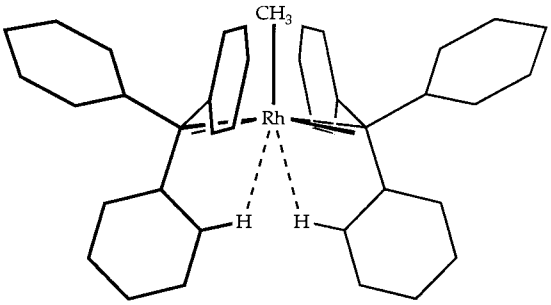

Fig. 2. Agostic *ortho*-CH…Rh bonding in $RhI_2(CH_3)(PPh_3)_2$(Rh…H = 3.33 Å).

evident in the solid state. A similar situation was found in **1**, fluxional at room temperature between two enantiomeric *nido* forms via an intermediate with overall C_s symmetry [2,3]. From VT ^{31}P NMR experiments $\Delta G\ddagger$ for this process in **1** is calculated to be 58 kJ mol^{-1}, and the measured coalescence temperature is 338 K. Similarly, cooling a $CDCl_3$ solution of **2** to 223 K arrests the fluxionality, with two doublets of doublets observed in the ^{31}P{^{1}H} NMR spectrum at δ 67.1 ppm [J(PP) 25, J(RhP) 142 Hz] and δ 51.0 ppm [J(PP) 25, J(RhP) 133 Hz]. For **2** $\Delta G\ddagger$ is calculated to be 46 kJ mol^{-1}, with the coalescence temperature 273 K, substantially lower than that in **1**.

Our next target {RhL_2} fragment was {Rh[$P(OMe)_3$]$_2$}, the rationale here being that γ-agostic bonding would be unlikely. Reaction between Cs[6-*arachno*-SB_9H_{12}] and one equivalent of ″RhCl[$P(OMe)_3$]″$_2$, generated in situ by reaction between [RhCl(η^2,η^2-C_8H_{12})]$_2$ and $P(OMe)_3$, resulted in the isolation of a bright yellow crystalline product in moderate yield (< 50%, after work-up), subsequently identified as 8,8,8-{$P(OMe)_3$}$_3$-8,7-*nido*-$RhSB_9H_{10}$, **3**, by microanalysis and multinuclear NMR spectroscopy. Thus in the ^{11}B{^{1}H} NMR spectrum are eight resonances between δ 16 and −26 ppm, the range associated with *nido*-MSB_9 fragments [2,3]. The ^{31}P{^{1}H} NMR spectrum of **3** reveals *three* different phosphorus environments, all displaying ^{103}Rh–^{31}P coupling, at δ = 141.6 [J(Rh–P) 205], 125.2 [J(Rh–P) 195] and 121.9 ppm [J(Rh–P) 129 Hz]. The two highest frequency resonances also show ^{31}P–^{31}P coupling, whilst the lowest frequency resonance is broadened to such an extent that only the Rh–P coupling is resolved. By analogy with the related trisphosphine species 8,8,8-$(PMe_2Ph)_3$-8,7-*nido*-$RhSB_9H_{10}$ in which the Rh–P bond *trans* to B(9) is significantly the longest [36], we assign the broad, lowest frequency, ^{31}P resonance in **3**, having substantially the smallest Rh–P coupling constant, as arising from a similarly disposed P atom.

The isolation of **3** as a trisphosphite compound was unplanned, but may be understood by the inability of

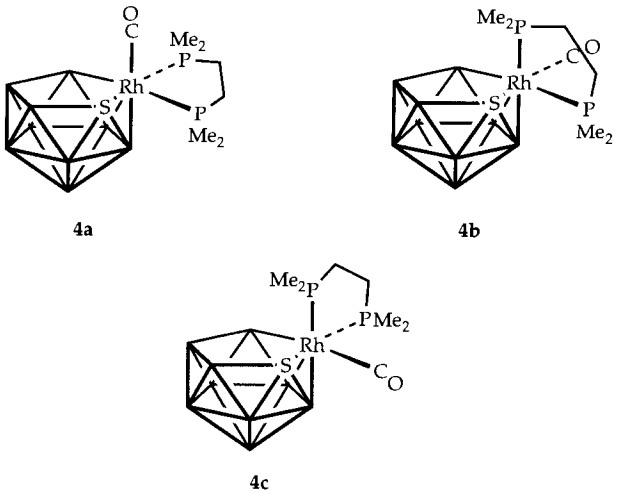

Fig. 3. Possible rotamers of compound **4**.

the phosphite ligands to stabilise '$\{P(OMe)_3\}_2$-$RhSB_9H_{10}$' by agostic bonding, resulting in the scavenging of a further equivalent of $P(OMe)_3$.

Consistent with this, reaction between Cs[6-*arachno*-SB_9H_{12}] and RhCl(dmpe)CO, the latter prepared by bridge cleavage of $[RhCl(CO)_2]_2$ with dmpe, did not result in CO loss but in formation of the new rhodathiaborane 8,8-(dmpe)-8-(CO)-8,7-*nido*-$RhSB_9H_{10}$, **4**, after work up by column chromatography. The IR spectrum of **4** shows an intense CO stretching band at 2039 cm^{-1} as well as a broad, medium intensity band, at 2530 cm^{-1}, due to B–H stretch. The $^{31}P\{^1H\}$ NMR spectrum of **4** reveals four resonances (all showing rhodium coupling) of approximately equal integral, two at relatively high frequency (45–50 ppm) and two at relatively low frequency (ca. 29 ppm, overlapping). In the $^{11}B\{^1H\}$ NMR spectrum there are 12 peaks between δ 15 and −29 ppm. We interpret these data as suggesting that **4** exists as a mixture of two of three possible rotamers, **4a**–**4c** (Fig. 3).

Single crystals of **4** were grown by the slow diffusion of a CH_2Cl_2 solution and 60–80°C light petroleum. Analysis of low-temperature diffraction data collected reveals that, in the crystal, **4** is a mixture of rotamers **4b** and **4c** (ca. 2:1 respectively), since positions 7 and 9 of the cage are mutually disordered. Redissolution of these crystals in $CDCl_3$ affords a ^{31}P NMR spectrum essentially identical to that previously obtained. Fig. 4 shows a perspective view of a single molecule of the major rotamer **4b**, and Table 6 lists selected molecular parameters determined.

Clearly, **4** displays the *nido* molecular structure anticipated by Wade's rules, the rhodium atom being exo-polyhedrally co-ordinated to dmpe and the carbon monoxide ligand. Because of the crystallographic disorder a detailed discussion of the molecular parameters in **4** is not appropriate. Briefly, then, the rhodium has a *pseudo*-octahedral co-ordination geometry, with bond lengths and angles being within the expected ranges. The Rh–P distance mainly trans to S, Rh(8)–P(1), is shorter than that mainly *cis*, Rh(8)–P(2), as found in 8,8,8-$(PMe_2Ph)_3$-8,7-*nido*-$RhSB_9H_{10}$ [36]. Unambiguous Rh to B distances, Rh(8)–B(3,4), compare well

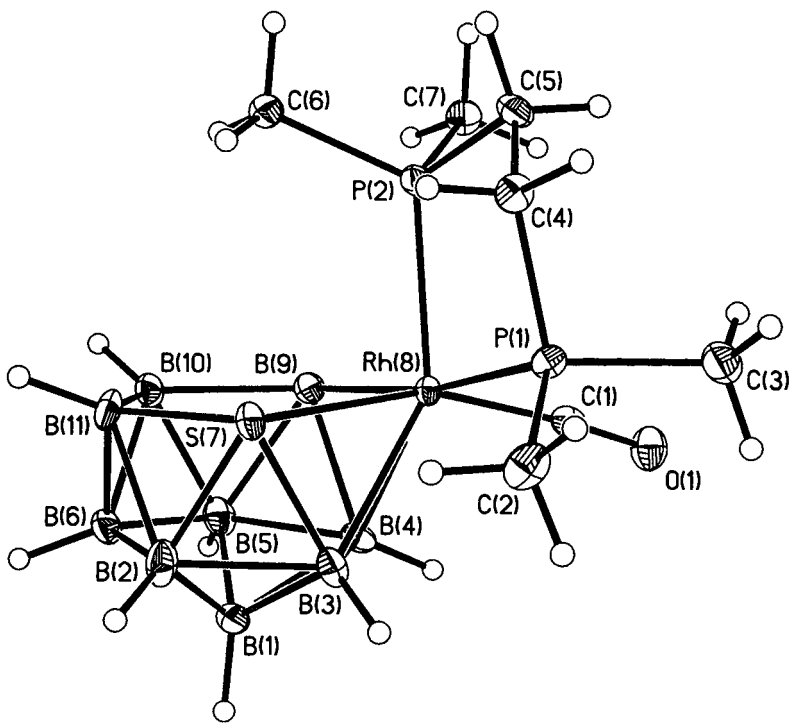

Fig. 4. Perspective view of the major rotamer **b** of compound **4** in the crystal. Thermal ellipsoids are drawn at the 40% probability level.

Table 6
Selected interatomic distances (Å) and interbond angles (°) in compound **4**

Rh(8)–C(1)	1.907(5)	Rh(8)–B(4)	2.256(5)
Rh(8)–B(3)	2.260(5)	Rh(8)–P(1)	2.3352(13)
Rh(8)–P(2)	2.3510(13)	Rh(8)–S(7)	2.364(2)
Rh(8)–B(9)	2.379(2)	P(2)–C(7)	1.817(4)
P(2)–C(6)	1.818(4)	P(2)–C(5)	1.841(5)
P(1)–C(2)	1.805(4)	P(1)–C(3)	1.822(5)
P(1)–C(4)	1.843(4)	S(7)–B(11)	1.914(5)
S(7)–B(2)	1.920(6)	S(7)–B(3)	2.003(6)
B(9)–B(5)	1.869(6)	B(9)–B(10)	1.911(6)
B(9)–B(4)	1.954(6)	O(1)–C(1)	1.135(5)
B(1)–B(2)	1.760(9)	B(1)–B(3)	1.765(8)
B(1)–B(4)	1.769(8)	B(1)–B(6)	1.778(8)
B(1)–B(5)	1.784(8)	B(2)–B(6)	1.766(8)
B(2)–B(11)	1.828(8)	B(2)–B(3)	1.855(8)
B(3)–B(4)	1.806(8)	B(4)–B(5)	1.838(8)
B(5)–B(6)	1.768(8)	B(5)–B(10)	1.800(8)
B(6)–B(11)	1.740(8)	B(6)–B(10)	1.746(7)
B(10)–B(11)	1.812(8)		
C(1)–Rh(8)–P(1)	88.86(14)	C(1)–Rh(8)–P(2)	103.24(14)
P(1)–Rh(8)–P(2)	84.61(5)	C(7)–P(2)–Rh(8)	117.4(2)
C(6)–P(2)–Rh(8)	116.9(2)	C(5)–P(2)–Rh(8)	107.7(2)
C(2)–P(1)–Rh(8)	120.2(2)	C(3)–P(1)–Rh(8)	117.4(2)
C(4)–P(1)–Rh(8)	106.00(14)	O(1)–C(1)–Rh(8)	175.4(4)
B(11)–S(7)–Rh(8)	110.6(2)	S(7)–Rh(8)–B(9)	91.04(8)
Rh(8)–B(9)–B(10)	109.3(2)	B(11)–B(10)–B(9)	115.2(3)
B(10)–B(11)–S(7)	113.4(3)		

between the two compounds, but the disorder means that in **4** Rh–S(7) is shorter, and Rh–B(9) longer, than in the tris(dimethylphenylphoshine) analogue. [3]

Our analyses of the structures of the 'rule-breaking' rhodaheteroboranes **1**, **2** and **8** has identified weak agostic *ortho*-CH · · · Rh bonding which supplies the metal centre with a net additional electron pair. Although there is precedent in the literature for agostic interactions involving *ortho*-phenyl hydrogen atoms [26–30], it is of relevance that they have never been identified spectroscopically in solution, and we have been similarly unsuccessful in observing the agostic interactions in **2** by NMR techniques. However, strong indirect evidence for these interactions derives from the structural consequences of deprotonation of the cage, as discussed in Section 3.3.

3.3. Deprotonation and reprotonation reactions

The *nido* species **1** and **2** both contain an (acidic) μ-H atom bridging the B(9)–B(10) polyhedral edge. We have considered the possibility that the formation of anionic rhodathiaboranes by removal of this bridge proton might disfavour the agostic *ortho*-CH · · · Rh interactions and result in the formation of *closo* products.

Treatment of compound **2** or **1** with one equivalent of MeLi at 195 K in THF followed by warming to room temperature afforded good yields of $[1,1\text{-(dppe)-}1,2\text{-}closo\text{-Rh-}SB_9H_9]^-$, **5**, or $[1,1\text{-}(PPh_3)_2\text{-}1,2\text{-}closo\text{-}RhSB_9H_9]^-$, **6**, respectively, isolated either by addition of 12-crown-4 to co-ordinate Li^+ (anion **5**) or by metathesis (anions **5** and **6**). The structural change occurring on deprotonation of **2** or **1** is readily demonstrated by the $^{11}B\{^1H\}$ NMR spectra of **5** and **6**. Thus **5** shows six resonances (1:1:2:1:2:2) between δ 59 and -30 ppm, whilst for **6** there are five resonances (1:1:3:2:2; underlined resonance a $2+1$ co-incidence) between δ 55 and -32 ppm. This chemical shift range is diagnostic of a *closo*-MSB_9 polyhedron [2,3] and the number and multiplicity of resonances implies C_s molecular symmetry. The $^{31}P\{^1H\}$ NMR spectra of **5** and **6** each reveal only a single ^{31}P environment, δ 69.4 [J(RhP) 155] for **5** and δ 44.9 [J(RhP) 154 Hz] for **6**. To confirm the molecular structure of these anions an X-ray diffraction study of [PPN]**5** was undertaken on crystals grown from MeCN–Et_2O, and subsequently shown to be the 0.5 MeCN solvate.

Fig. 5 shows the molecular structure of **5** and the numbering scheme employed, whilst Table 7 lists selected interatomic distances and angles. Immediately apparent is that **5** has a *closo* 11-vertex molecular architecture with effective C_s symmetry about the plane defined by Rh(1)S(2)B(3)B(8)B(9), fully consistent with the NMR data. The RhP_2 plane is orthogonal to the former plane, with a dihedral angle of 89.9°. The Rh-p distances are 2.242(3) and 2.259(3) Å, somewhat shorter than in 1-(CO)-1,3-$(PMe_2Ph)_2$-*closo*-1,2-$RhSB_9H_8$, the only comparable molecule in the literature [2,3]. Rh–S is 2.378(3) Å and Rh–B distances span the range 2.169(11)–2.455(11) Å. There are no Rh . . . H distances <3.3 Å.

Thus anions **5** and **6** are closed rhodathiaboranes with polyhedral geometries based on an octadecahedron. Clearly a major structural change has been effected by the deprotonation of compounds **2** and **1**, with anion formation resulting in the *ortho*-CH · · · Rh agostic interactions being 'switched off' to afford *closo* polyhedra which obey Wade's rules. The $\{SB_9H_9\}$ subclusters of **5** and **6** carry formal charges of -2, leading to the conclusion that the structural change upon deprotonation of **2** and **1** has been accompanied by a reduction in the formal oxidation state of rhodium from $+3$ to $+1$.

Interestingly, this structural change is fully reversible. Thus, addition of one drop of HBF_4 to a CD_2Cl_2 solution of [PPN]**5** immediately regenerates compound **2** in essentially quantitative yield by ^{11}B and

[3] Surprisingly, in **4** the Rh(8)–S(7) distance appears to be actually shorter than Rh(8)–B(9), by 0.015(3) Å, which might imply that the relative occupations of the disordered positions 7 and 9 were incorrect. However, sensible thermal parameters for atoms at positions 7 and 9 were only obtained with the former being mainly sulfur.

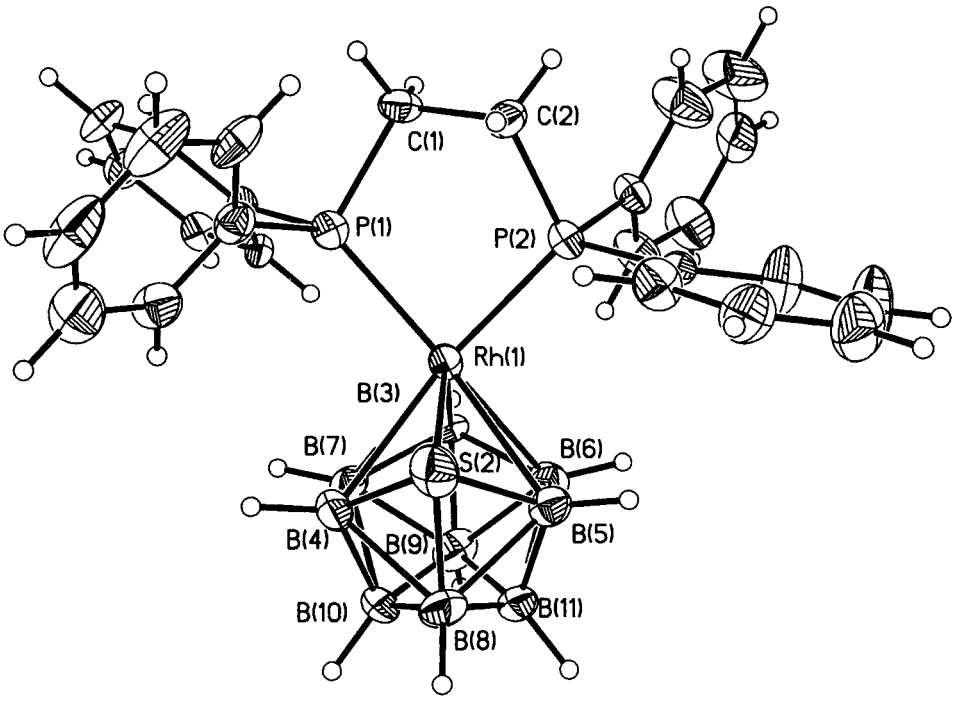

Fig. 5. Perspective view of the anion **5** with atom labelling. Thermal ellipsoids at 40% probability level.

^{11}H NMR spectroscopy (Scheme 1). However, in co-ordinating solvents adducts of the original neutral species are formed (Scheme 2). Thus, treatment of a MeCN solution of [Li(12-crown-4)$_2$]**5** with CF_3CO_2H affords the new thiaborane 8,8-(dppe)-8-(MeCN)-8,7-*nido*-$RhSB_9H_{10}$, **7**, in good yield. The identity of **7** was established by microanalysis and multinuclear NMR spectroscopy. The $^{11}B\{^1H\}$ NMR spectrum of **7** reveals seven resonances in the ratio 2:2:1:1:1:1:1 (the first two signals co-incident) between δ 11 ppm and −25 ppm, a typical *nido*-MSB_9 shielding pattern. As well as signals due to dppe, the ^{1}H NMR spectrum displays a sharp singlet integrating for three protons at δ 2.48 ppm, assigned to co-ordinated acetonitrile. In the $^{31}P\{^1H\}$ NMR spectrum are only two signals, showing that only one of the three possible rotamers is formed (cf. Fig. 3).

Table 7
Selected interatomic distances (Å) and interbond angles (°) in [PPN]**5** ·0.5 MeCN

Rh(1)–P(2)	2.242(3)	Rh(1)–P(1)	2.259(3)
Rh(1)–S(2)	2.378(3)	Rh(1)–B(3)	2.169(11)
Rh(1)–B(4)	2.455(11)	Rh(1)–B(5)	2.390(12)
Rh(1)–B(6)	2.336(13)	Rh(1)–B(7)	2.398(12)
S(2)–B(4)	1.924(13)	S(2)–B(5)	1.934(12)
S(2)–B(8)	1.97(2)	B(3)–B(9)	1.66(2)
B(3)–B(7)	1.73(2)	B(3)–B(6)	1.73(2)
B(4)–B(10)	1.76(2)	B(4)–B(7)	1.83(2)
B(4)–B(8)	1.88(2)	B(5)–B(11)	1.78(2)
B(5)–B(6)	1.84(2)	B(5)–B(8)	1.88(2)
B(6)–B(9)	1.77(2)	B(6)–B(11)	1.80(2)
B(7)–B(10)	1.79(2)	B(7)–B(9)	1.80(2)
B(8)–B(11)	1.72(2)	B(8)–B(10)	1.72(2)
B(9)–B(11)	1.78(2)	B(9)–B(10)	1.79(2)
B(10)–B(11)	1.80(2)	P(1)–C(21)	1.827(5)
P(1)–C(1)	1.847(9)	P(1)–C(11)	1.849(6)
P(2)–C(2)	1.816(10)	P(2)–C(41)	1.837(5)
P(2)–C(31)	1.843(6)	P(3)–N(1)	1.558(9)
P(3)–C(111)	1.787(6)	P(3)–C(121)	1.790(6)
P(3)–C(101)	1.821(6)	P(4)–N(1)	1.579(8)
P(4)–C(211)	1.794(6)	P(4)–C(201)	1.795(5)
P(4)–C(221)	1.796(6)		
P(2)–Rh(1)–P(1)	85.16(11)	C(21)–P(1)–C(1)	101.2(4)
C(21)–P(1)–C(11)	100.4(3)	C(1)–P(1)–C(11)	103.5(4)
C(21)–P(1)–Rh(1)	123.1(3)	C(1)–P(1)–Rh(1)	109.1(3)
C(11)–P(1)–Rh(1)	116.9(2)	C(2)–P(2)–C(41)	102.2(4)
C(2)–P(2)–C(31)	103.3(4)	C(41)–P(2)–C(31)	102.2(3)
C(2)–P(2)–Rh(1)	109.5(3)	C(41)–P(2)–Rh(1)	121.3(3)
C(31)–P(2)–Rh(1)	116.1(3)	P(3)–N(1)–P(4)	146.7(6)

The molecular structure of **7**, and thus the identity of this single rotamer, was established by crystallographic study of the MeCN solvate, crystals having been grown from MeCN solution. Fig. 6 presents a perspective view of a single molecule, and pertinent distances and angles are contained within Table 8. Clearly, the overall structural motif is *nido*, fully consistent with electron counting rules. The acetonitrile ligand lies trans to B(9), thus identifying the single rotamer of **7** as being that which corresponds to **4c**. Rh–P distances are 2.291(2) and 2.353(2) Å, similar to those found in 8,8,8-(PMe_2Ph)-8,7-*nido*-$RhSB_9H_{10}$ [36], with the shorter distance of each pair belonging to the phosphorus atom lying *trans* to S(7). Rh–B distances are 2.219(11) and 2.266(10) Å to B(4) and B(3), respectively, fully comparable with the equivalent distances in 8,8,8-(PMe_2Ph)-8,7-*nido*-$RhSB_9H_{10}$. However, Rh(8)–B(9) in **7** is relatively short, 2.154(11) Å, presumably reflecting the differing trans influences of MeCN and PMe_2Ph. The acetonitrile

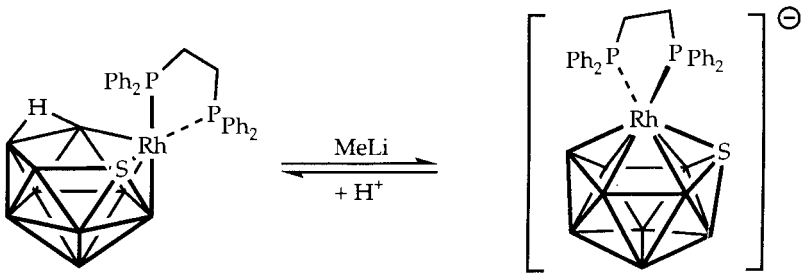

Scheme 1.

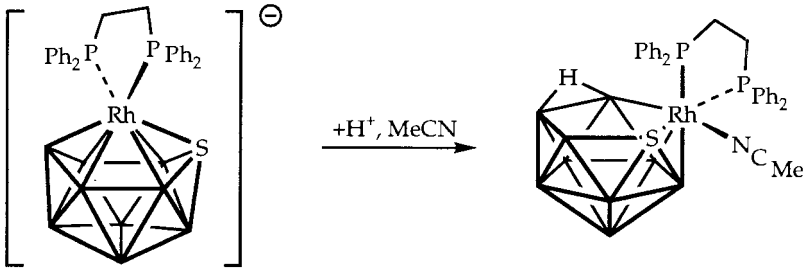

Scheme 2.

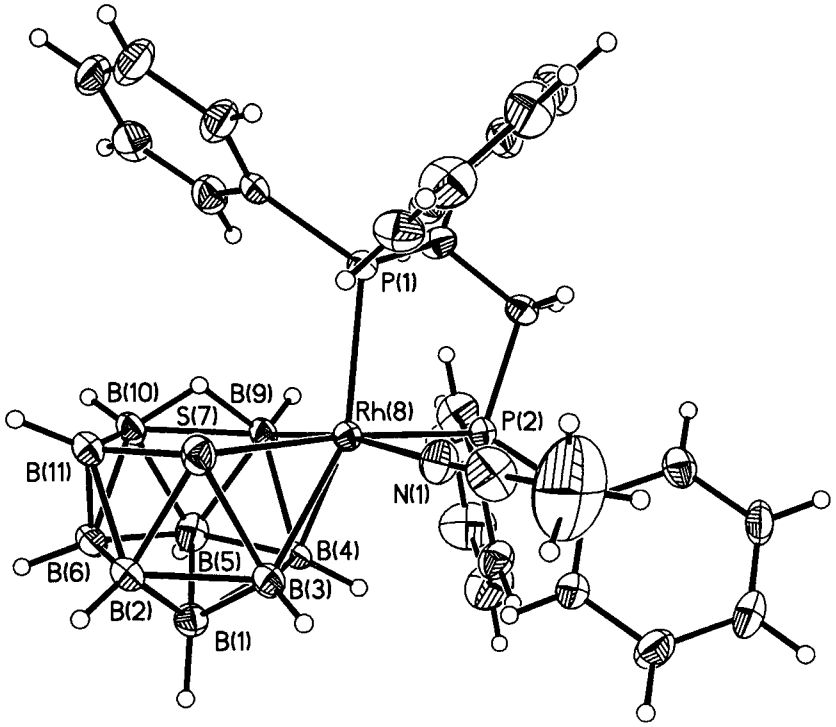

Fig. 6. Perspective view (40% probability ellipsoids) of compound **7** with key atoms labelled.

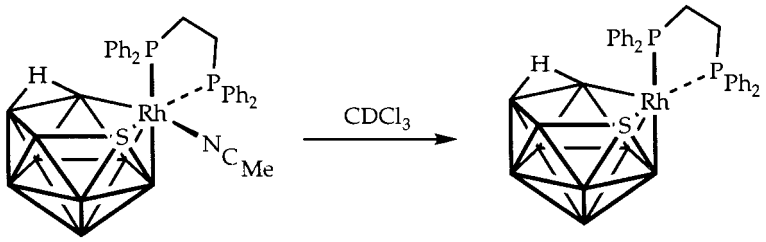

Scheme 3.

Table 8
Selected interatomic distances (Å) and interbond angles (°) in compound **7**

P(1)–Rh(8)	2.353(2)	P(2)–Rh(8)	2.291(2)
N(1)–Rh(8)	2.206(8)	B(3)–Rh(8)	2.266(10)
B(4)–Rh(8)	2.219(11)	S(7)–Rh(8)	2.368(2)
Rh(8)–B(9)	2.154(11)	P(1)–C(11)	1.822(10)
P(1)–C(41)	1.827(9)	P(1)–C(1)	1.838(9)
P(2)–C(31)	1.819(9)	P(2)–C(21)	1.842(10)
P(2)–C(2)	1.844(9)	N(1)–C(3)	1.101(14)
C(1)–C(2)	1.524(12)	B(1)–B(2)	1.75(2)
B(1)–B(4)	1.777(14)	B(1)–B(3)	1.78(2)
B(1)–B(6)	1.79(2)	B(1)–B(5)	1.79(2)
B(2)–B(6)	1.76(2)	B(2)–B(11)	1.82(2)
B(2)–B(3)	1.90(2)	B(2)–S(7)	1.992(11)
B(3)–B(4)	1.80(2)	B(3)–S(7)	2.090(12)
B(4)–B(5)	1.774(14)	B(4)–B(9)	1.852(14)
B(5)–B(6)	1.77(2)	B(5)–B(9)	1.79(2)
B(5)–B(10)	1.81(2)	B(6)–B(11)	1.73(2)
B(6)–B(10)	1.749(14)	S(7)–B(11)	1.906(12)
B(9)–B(10)	1.894(14)	B(10)–B(11)	1.84(2)
P(2)–Rh(8)–P(1)	85.65(8)	N(1)–Rh(8)–P(1)	94.3(2)
N(1)–Rh(8)–P(2)	91.0(2)	C(11)–P(1)–Rh(8)	116.8(3)
C(41)–P(1)–Rh(8)	120.6(3)	C(1)–P(1)–Rh(8)	104.7(3)
C(31)–P(2)–Rh(8)	114.0(3)	C(21)–P(2)–Rh(8)	122.3(3)
C(2)–P(2)–Rh(8)	106.9(3)	C(3)–N(1)–Rh(8)	177.0(10)
N(1)–C(3)–C(4)	178(2)	B(11)–S(7)–Rh(8)	110.4(4)
B(9)–Rh(8)–S(7)	90.2(3)	B(10)–B(9)–Rh(8)	116.5(6)
B(11)–B(10)–B(9)	110.5(7)	B(10)–B(11)–S(7)	111.6(6)

ligand is essentially linear, N(1)–C(3)-C(4) 178(2)°, with the Rh–N bond length being 2.206(8) Å.

If a $CDCl_3$ solution of **7** is allowed to stand at room temperature for ca. 24 h, compound **2** and free acetonitrile are regenerated virtually quantitatively, identified by ^1H, ^{31}P and ^{11}B NMR spectroscopy (Scheme 3). This demonstrates that the agostic interactions in **2**, although presumably weak, are nevertheless sufficiently strong to displace MeCN from the rhodium co-ordination sphere.

4. Conclusions

The $RhSB_9$ and RhC_2B_8 heteroboranes are extremely interesting. Compounds **1** and **8** have both been described [2,3,14] as constituting exceptions to Wade's rules, although the 'anomalous' structure of **8** was rationalised by a modification to the electron counting convention suggested by Nishimura.[4] We have confirmed that **1** and **8** have *nido* structures by RMS misfit calculations, but we have identified that these species have access to an additional SEP via *ortho*-CH · · · Rh agostic interactions, and so do not contravene Wade's rules.

The overall area is quite complex. Thus, the agostic bonding in **1** can be displaced by small 2-*e* donors (CO, CS_2) or the entire *exo*-polyhedral ligand set can be substituted by three phosphines with smaller cone angles [2,3]. When we have attempted to prepare compounds similar to **1** but which are denied agostic bonding we have found either decomposition, the formation of direct analogues (e.g., **2**), ligand scavenging (e.g., in **3**), retention of potentially labile ligands (e.g., in **4**) or the formation of bimetallic products accompanied by ligand scavenging [37].

In contrast, the *nido* species $(PEt_3)_3RhC_2B_8H_{11}$ reversibly dissociates PEt_3 to afford the triethylphosphine analogue of **8** which then converts to the *closo* hydrido species $(PEt_3)_2Rh(H)C_2B_8H_{10}$ [14]. We have never seen evidence for metal hydrides in the rhodathiaborane system, but we are were able to produce *closo* products (e.g., **5** and **6**) by deprotonation reactions which (reversibly) switch-off the agostic bonding. Reprotonation in MeCN has afforded a tris ligand species (**7**) but this reverts to the agostically-stabilised **2** on standing in $CDCl_3$.

In all the above cases where molecular structures are confirmed, Wade's rules hold. It has long been our contention that apparent exceptions to Wade's rules should be very carefully considered before being claimed as anomalous.

References

[1] K. Wade, J. Chem. Soc., Chem. Commun. (1971) 792.
[2] G. Ferguson, M.C., Jennings, A.J. Lough, S. Coughlan, T.R. Spalding, J.D. Kennedy, X.L.R. Fontaine, B. Stibr, J. Chem. Soc., Chem. Commun. (1990) 891.

[4] E.K. Nishimura, personal communication to M.F. Hawthorne, referenced in Ref. [14].

[3] S. Coughlan, T.R. Spalding, G. Ferguson, J.F. Gallagher, A.J. Lough, X.L.R. Fontaine, J.D. Kennedy, B. Stibr, J. Chem. Soc., Dalton Trans. (1992) 2865.
[4] M. Murphy, T.R. Spalding, G. Ferguson, J.F. Gallagher, Acta Crystallogr. C48 (1992) 638.
[5] S.A. Macgregor, A.J. Wynd, N. Moulden, R.O. Gould, P. Taylor, L.J. Yellowlees, A.J. Welch, J. Chem. Soc., Dalton Trans. (1991) 3317.
[6] K.J. Adams, T.D. McGrath, Rh.Ll Thomas, A.S. Weller, A.J. Welch, J. Organomet. Chem. 527 (1997) 283.
[7] G. Giordano, R.H. Crabtree, Inorg. Synth. 19 (1979) 218.
[8] R. Cramer, Inorg. Synth. 15 (1974) 17.
[9] R. Cramer, Inorg. Synth. 15 (1974) 15.
[10] R.W. Rudolph, W.R. Pretzer, Inorg. Synth. 22 (1982) 226.
[11] J.W. Pflugrath, A. Messerschmidt, MADNES, Version EEC 11/09/89. Munich Area Detector (New EEC) System, Enraf–Nonius, Delft, The Netherlands, 1991.
[12] N.G. Walker, D. Stuart, Acta Crystallogr. A39 (1983) 158.
[13] G.M. Sheldrick, SHELXTL/PC, Version 5.0, Siemens Analytical X-ray Instruments, Madison, WI, USA, 1994.
[14] C.W. Jung, M.F. Hawthorne, J. Am. Chem. Soc. 102 (1980) 3024.
[15] P. Lu, C.B. Knobler, M.F. Hawthorne, Acta Crystallogr. C40 (1984) 1704.
[16] G.K. Barker, M. Green, F.G.A. Stone, A.J. Welch, W.C. Wolsey, J. Chem. Soc., Chem. Commun. (1980) 627.
[17] M.I. Forsyth, D.M.P. Mingos, A.J. Welch, J. Chem. Soc., Dalton Trans. (1978) 1363.
[18] P.T. Brain, M. Bühl, J. Cowie, Z.G. Lewis, A.J. Welch, J. Chem. Soc., Dalton Trans. (1996) 231.
[19] T.D. Getman, J.A. Krause, S.G. Shore, Inorg. Chem. 27 (1988) 2398.
[20] T.D. McGrath, A.J. Welch, Acta Crystallogr. C53 (1997) 229.
[21] J. Buchanan, E.J.M. Hamilton, D. Reed, A.J. Welch, J. Chem. Soc., Dalton Trans. (1990) 677.
[22] R. Brill, H. Dietrich, H. Dierks, Acta Crystallogr. B27 (1971) 2003.
[23] R.L. Ernst, W. Quintana, R. Rosen, P.J. Carroll, L.G. Sneddon, Organometallics 6 (1987) 80.
[24] T.D. McGrath, PhD Thesis, University of Edinburgh, 1994.
[25] F.A. Cotton, G. Wilkinson, Advanced Inorganic Chemistry, 5th edn., Wiley, New York, USA, 1988.
[26] S.J. LaPlaca, J.A. Ibers, Inorg. Chem. 4 (1965) 778.
[27] A.C. Skapski, P.G.H. Troughton, J. Chem. Soc., Chem. Commun. (1968) 1230.
[28] R.-M. Catalá, D. Cruz-Garritz, P. Sosa, P. Terreros, H. Torrens, A. Hills, D.L. Hughes, R.L. Richards, J. Organomet. Chem. 359 (1989) 219.
[29] S.D. Chappell, L.M. Engelhardt, A.H. White, C.L. Raston, J. Organomet. Chem. 462 (1993) 295.
[30] S.D. Perera, B.L. Shaw, J. Chem. Soc., Dalton Trans. (1995) 3861.
[31] W.A. King, X.-L. Luo, B.L. Scott, G.J. Kubas, K.W. Zilm, J. Am. Chem. Soc. 118 (1996) 6782.
[32] A.R. Siedle, R.A. Newmark, L.H. Pignolet, Organometallics 3 (1984) 855.
[33] P. Albano, M. Aresta, M. Manassero, Inorg. Chem. 19 (1980) 1069.
[34] K.J. Adams, T.D. McGrath, A.J. Welch, Acta Crystallogr. C51 (1995) 401.
[35] G.M. Rosair, A.J. Welch, A.S. Weller, Acta Crystallogr. C52 (1996) 3020.
[36] G. Ferguson, A.J. Lough, S. Coughlan, T.R. Spalding, Acta Crystallogr. C48 (1992) 440.
[37] K.J. Adams, T.D. McGrath, A.J. Welch, Polyhedron, in press (paper 97-120).